BJR

Received: 10 June 2014 | Revised: 28 October 2014 | Accepted: 6 November 2014

doi: 10.1259/bjr.20140418

Cite this article as:
Yu TG, Feng Y, Feng XY, Dai JZ, Qian HJ, Huang Z. Prognostic factor from MR spectroscopy in rat with astrocytic tumour during radiation therapy. Br J Radiol 2015;88:20140418.

FULL PAPER

Prognostic factor from MR spectroscopy in rat with astrocytic tumour during radiation therapy

[1]T G YU, MD, [2]Y FENG, PhD, [1]X Y FENG, MD, [1]J Z DAI, MD, [3]H J QIAN, MD and [2]Z HUANG, PhD

[1]Department of Radiology, Huashan Hospital, Fudan University, Shanghai, China
[2]Department of Radiation Oncology, East Carolina University, Greenville, NC, USA
[3]Department of Radiology, Obstetrics and Gynecology Hospital, Fudan University, Shanghai, China

Address correspondence to: Dr Zhibin Huang
E-mail: *huangz@ecu.edu*

Objective: To investigate the relationship between the tumour volume and metabolic rates of astrocytic tumours using MR spectroscopy (MRS) during radiation therapy (RT).
Methods: 12 healthy male Sprague-Dawley® rats (Sprague–Dawley Animal Company, Madison, WI) were used, and a tumour model was created through injecting C6 tumour cells into the right caudate nuclei of the rats. Tumours grew for 18 days after the injection and before the imaging study and radiation treatment. MRS was performed with two-dimensional multivoxel point-resolved spectroscopy sequence using a GE Signa VH/i 3.0-T MR scanner (GE Healthcare, Milwaukee, WI) equipped with rat-special coil. RT was given on the 19th day with a dose of 4 Gy in one single fraction. The image examinations were performed before RT, and on the 4th, 10th, 14th and 20th days after treatment, respectively. GE FuncTool software package (GE Healthcare) was used for post-processing of spectrum.
Results: Metabolic ratios of serial MRS decrease progressively with time after RT. Choline-containing components (Cho)/creatine and creatine phosphate (Cr) ratios immediately prior to RT differed significantly from those on the 10th, 14th and 20th days after RT; both Cho/*N*-acetyl aspartate (NAA) ratios and NAA/Cr ratios immediately prior to RT differed significantly from those on the 14th and 20th days after RT. A positive correlation between changes of tumour volume and changes of Cho/Cr, lipid and lactate/Cr and glutamate plus glutamine/Cr ratio was observed on the 4th day after RT.
Conclusion: MRS provides potential in monitoring tumour response during RT, and the imaging biomarkers predict the response of astrocytic tumours to treatment.
Advances in knowledge: MRS is combined with both tumour size and Ki-67 labelling index to access tumour response to radiation.

More than 180,000 brain tumours (malignant and benign) are diagnosed each year in the USA. Of these, about 23,380 are primary brain tumours.[1] Among the primary brain tumours, approximately 50% are glioblastoma multiform (GBM) and 50% are gliomas. Glioma has been thought of as a disease involving multiple gene mutations.[2] It has always been difficult for neurologists to diagnose and treat glioma, especially GBM.[3]

Although conventional MRI can be used to detect brain lesions, its sensitivity and specificity for distinguishing between benign and malignant lesions and differentiating between tumours and non-neoplastic lesions are limited. Similar MRI features may be present in several different tumour types. It is very difficult to differentiate high-grade and low-grade brain tumours with conventional MRI.[4]

The lack of biological markers with prognostic significance impedes the development of new treatment strategies. Although some biomarkers can be identified through molecular analysis[5] and DNA microarray,[6] these procedures normally require diagnostic biopsies that may not be feasible owing to tumour location. With the advancement of MR spectroscopy (MRS), biologically relevant intracellular metabolites can be detected, grading of astrocytomas can be assessed and their biological behaviour and prognosis can be evaluated.[7]

MRS is a unique method for performing analysis of the metabolism of organs and cells. It allows measurements of metabolites for specific atomic nuclei and their components, including choline-containing components (Cho), creatine and creatine phosphate (Cr), *N*-acetyl aspartate (NAA), lipid and lactate (LL) levels and glutamate plus glutamine (Glx). The most commonly studied metabolites in the brain are NAA, Cho and Cr.[8–12] NAA is a predictor for neuronal and axonal integrity since decreased levels are usually observed after brain injury. The second most

commonly observed MRS finding after brain tumours is increased Cho levels via cell membrane disruption and altered phospholipid metabolism,[13] which are biomarkers for cell membrane turnover.[14] The Cho level may be used to predict the malignancy of gliomas.[15] The Cho level has been found to correlate with the cellular density of tumours.[16] The Cr peak is an indicator of cell energy metabolism[17] and can be used to distinguish pure tumours from pure necrosis.[18] It has been found that Cho and LL levels normalized to Cr are a strong predictor of survival,[19] especially when diagnostic biopsies are not feasible. Glx changes arise from both neuronal and glial cells and reflect cytoplasmic concentrations.[20] The ratio of Glx/Cr was increased in 10 patients of brain tumour with oedema, which is associated with injury to the myelin sheath.[21] High Glx/Cr *in vivo* MRS index is a good predictor of tumour grading.[22] Significant correlations have been reported with hippocampal volumetric measures and Glx/Cr in patients with schizophrenia but not in healthy controls,[23] although the relationship between volume and Glx/Cr has been explored in brain tumours. Thus, MRS potentially shows promise in brain tumour management.

The Ki-67 labelling index (LI) is a promising proliferation marker in histological examination. Barbarella et al[24] first reported that the Ki-67 LI was correlated with Cho/Cr ratio. It is an independent predictor of both tumour recurrence and overall survival in meningioma.[25] It can be used to predict clinical outcome in acromegalic patients.[26] The Ki-67 LI increased at higher histological grades.[27] It is a reliable tool to accurately determine the growth fraction of neoplasms in humans and animals.[28] Therefore, it has been used to predict clinical outcome.

In this study, we tested our hypothesis that biomarkers illuminated by MRS during radiation therapy (RT), including NAA, Cho, LL and Glx/Cr, can add significant predictive power to clinical response to RT. We present the prognostic information on these biomarkers and demonstrate that these provide useful prognosis. We investigated the relationship between tumour volume and the metabolic ratios, including Cho/Cr, LL/Cr and Glx/Cr as well as the relationship between Ki-67 LI and the metabolic ratios of these.

METHODS AND MATERIALS

Animal model of C6 glioma

12 healthy male Sprague-Dawley® rats (Sprague–Dawley Animal Company, Madison, WI) weighing between 250 and 300 g (median weight, 275 g) were used in this study after approval by the Institutional Animal Care and Use Committee of Fudan University, Shanghai, China. They were fed and housed in the Huashan Hospital at the Fudan University under aseptic conditions. The tumour model was created by injecting cultured cells of C6 glioma cell line into the brain of the rats.

Cell culture

Astrocytic tumour C6 cells were provided by the Institute of Biochemistry and Cell Biology at the Shanghai Institute for Biological Sciences. C6 cells were cultured in McCoy's medium supplemented with 10% heat-inactivated foetal bovine serum, 100 U ml^{-1} penicillin and 100 μg ml^{-1} streptomycin. They were maintained as exponentially growing monolayers at 37 °C in a humidified atmosphere consisting of 95% air and 5% CO_2.

Intracranial injection of tumour cells

An hour before starting intracranial (IC) injection, C6 cells were washed once with phosphate-buffered saline solution, harvested by trypsinization, counted and resuspended in serum-free McCoy's medium to a final concentration of 1.2×10^6 cells per 10 μl. For IC injection, rats were anaesthetized by an intraperitoneal (IP) injection of a mixture of ketamine/xylazine (60/7.5 mg kg^{-1}, respectively). A volume of 10 μl of cell suspension was slowly injected into the right caudate–putamen of the animal's brain, as described in the literature.[29] Buprenorphine was injected subcutaneously right after the injection of tumour cells for optimal pain management (0.05 mg kg^{-1}; $v = 1$ ml).

Animal handling during MR acquisition

Animals were anaesthetized using a mixture of isoflurane in O_2 (3%, 1.5 ml min^{-1}). Then, they were placed on an electric heating pad and maintained under anaesthesia using a nose cone (1–2% isoflurane in O_2, 1.5 ml min^{-1}) throughout the imaging session. A 24-G catheter was secured into the animal's tail vein to allow for intravenous injection of hyperpolarized (1-^{13}C) pyruvate. Rats were placed in a custom-made cradle for positioning the brain in the centre of the radiofrequency (RF) coil and in the centre of a magnet. A water-heating pad was used to maintain stable body temperature of the animals throughout the imaging session.

Customized special coil for rats was configured by using a polyvinyl chloride pipe that is 15 cm in length and 6.4 cm in inner diameter, which was wound around eight units of birdcage coil. The solenoid coil had a diameter of 6.4 cm and a length of 10 cm and was placed in the RF shielding cylinder of 12 cm outside diameter. Since the coil requires much lower energy than the conventional 3-T MR head coil, we reduced transmit signals by 20 db through an attenuator. Therefore, automatic scanning software can be used to correct the energy transmitted to the RF receiver as well as the gain received by the RF receiver.

Rat irradiation

The tumour model was created successfully in 18 days after the implantation. The 12 rats were then treated with primary RT, which included external beam RT with 6-MV photons (a total of 4 Gy in one single fraction delivered to the head region of 2 × 2 cm between the anterior-bottom edges of both eyes and anterior-bottom edges of both ears) using a clinical linear accelerator (CLINAC-600C; Varian Medical Systems, Palo Alto, CA). The machine used in our study was equipped with a collimator of 120 leaves, which can create a maximal field size of 40 × 40 cm with 0.5-cm leaves in the central 20 × 20-cm region and 1-cm leaves in the outer 20-cm field. Irradiation to the rats was performed with the central field within 20 × 20 cm region. And to minimize the impact of leaf width, we designed the two-dimensional (2D) treatment plans through rotating the collimator such that the ends of the leaves (rather than the sides of leaves) were used to conform the treatment fields to the tumour. Figure 1 shows the isodose distributions of a treatment plan for a rat brain tumour.

Figure 1. Isodose distributions of a treatment plan for a rat brain using the central part of leaves with width of 0.5 cm. Tumour was contoured in yellow. The prescription lines are 100% (4 Gy) in red, 80% in green, 50% in light blue and 30% in blue. For colour images see online: www.birpublications.org/doi/abs/10.1259.bjr.20140418.

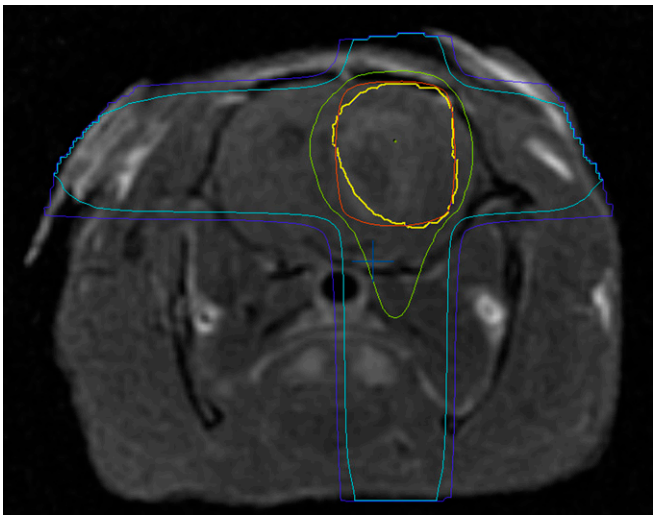

MRI protocol, MR spectroscopy and tumour volume measurement

Conventional MRI

All rats were examined using the 3.0-T MRI/MRS scanner (GE Healthcare, Milwaukee, WI). Conventional MR sequences were as follows: sagittal fast spin-echo T_1 weighted imaging for location; axial spin echo T_1 weighted imaging [repetition time (TR)/echo time (TE) = 400/11 ms; field of view (FOV) = 60 mm; matrix = 256 × 256; number of excitation pulses = 2; bandwidth = 12.5 kHz; slice thickness = 1 mm; interslice gap = 0.2 mm; total number of scan slices = 16]; fast spin echo T_2 weighted imaging (TR/TE = 4000/120 ms; other parameters identical to those used in the T_1 weighted spin echo sequence); and fast fluid attenuation inversion recovery (TR/TE = 4000/120 ms; time of inversion = 2200 ms; matrix = 256 × 192; number of excitation pulses = one; other parameters identical to those used in the T_1 weighted spin-echo sequence).

MR spectroscopy

For all rats, an automated multivoxel 2D chemical shift imaging sequence (TR = 1000 ms; TE = 35 ms; phase encoding $x = 24$; phase encoding $y = 24$; number of excitation pulses = one) was used for ^{1}H-MRS, and contralateral normal brain tissue was used as a control. FOV was 60 mm in diameter, slice thickness was 4 mm and the voxel size of the MRS was $1.87 \times 1.87 \times 4\ mm^3$. Tumour and ^{1}H-MRS were located by T_2 weighted imaging, and shimming was performed by the MRI scanner automatically. The volume of interest was chosen within the solid tumour so as to avoid the strong interference from subcutaneous fat, haemorrhage, necrosis and the cystic part of the tumour. The total duration for 2D ^{1}H-MR spectrum acquisition was 580 s.

The noise level was estimated by computing the root-mean-square (RMS) noise values over two 2.35-ppm wide regions of the spectrum [the range of frequencies (−4.51 ppm, −2.16 ppm) and (2.86 ppm, 5.21 ppm)] and taking the greater of the two levels. If the quantitative analysis routine finds and fits a peak in a region, a failure is reported if the signal-to-noise ratio (SNR) of the peak is <5 to 1, and/or the goodness of fit of the peak is <4. The SNR is the usual signal-to-noise ratio; the noise is estimated by taking the average RMS value over two regions of data. The goodness of fit is a ratio of the power of the peak (over the fitting region) *vs* the power of the residue. The power of the peak is taken to be the lesser of the power of the data over the region, and the power of the curve fit data over the region. If neither criterion is met, a failure is reported and "-ND-" (for not detected) is displayed for the peak values.

Table 1. Change in both tumour volume and metabolic ratio on the fourth day after radiation therapy (RT)

Rat	Volume (%)	Cho/Cr (%)	Cho/NAA (%)	NAA/Cr (%)	Lip0.9/Cr (%)	Lipid and lactate/Cr (%)	mI/Cr (%)	Glutamate plus glutamine/Cr (%)
1	+135	+7	+13	−5	+108	+52	+23	+70
2	−94	−31	−7	−26	+43	−27	+9	−47
3	−95	−22	−2	−21	+17	+17	+33	+40
4	−99	−10	−7	−4	+43	−30	+41	−17
5	−94	−11	+16	−24	+21	−54	−19	+17
6	+220	+57	+36	−24	+79	+118	−37	+75
7	−62	−30	−23	−9	+127	−4	−65	+16
8	−10	+31	+49	−12	+32	−23	+45	−14
9	−98	−49	−40	−14	−53	−84	−8	−56
10	−88	−45	−21	−30	−30	−84	−45	−44
11	−73	−41	+56	−62	−64	−68	−1	−25
12	+85	+10	+9	+1	+34	+273	+109	+50

Cho, choline-containing components; Cr, creatine and creatine phosphate; Lip0.9, lipid signal at 0.9 ppm; mI, myo-inositol; NAA, *N*-acetyl aspartate.

Figure 2. Change in tumour volume as well as the corresponding metabolites before radiation therapy (RT) and on the 4th, 10th, 14th and 20th days after RT initiation.

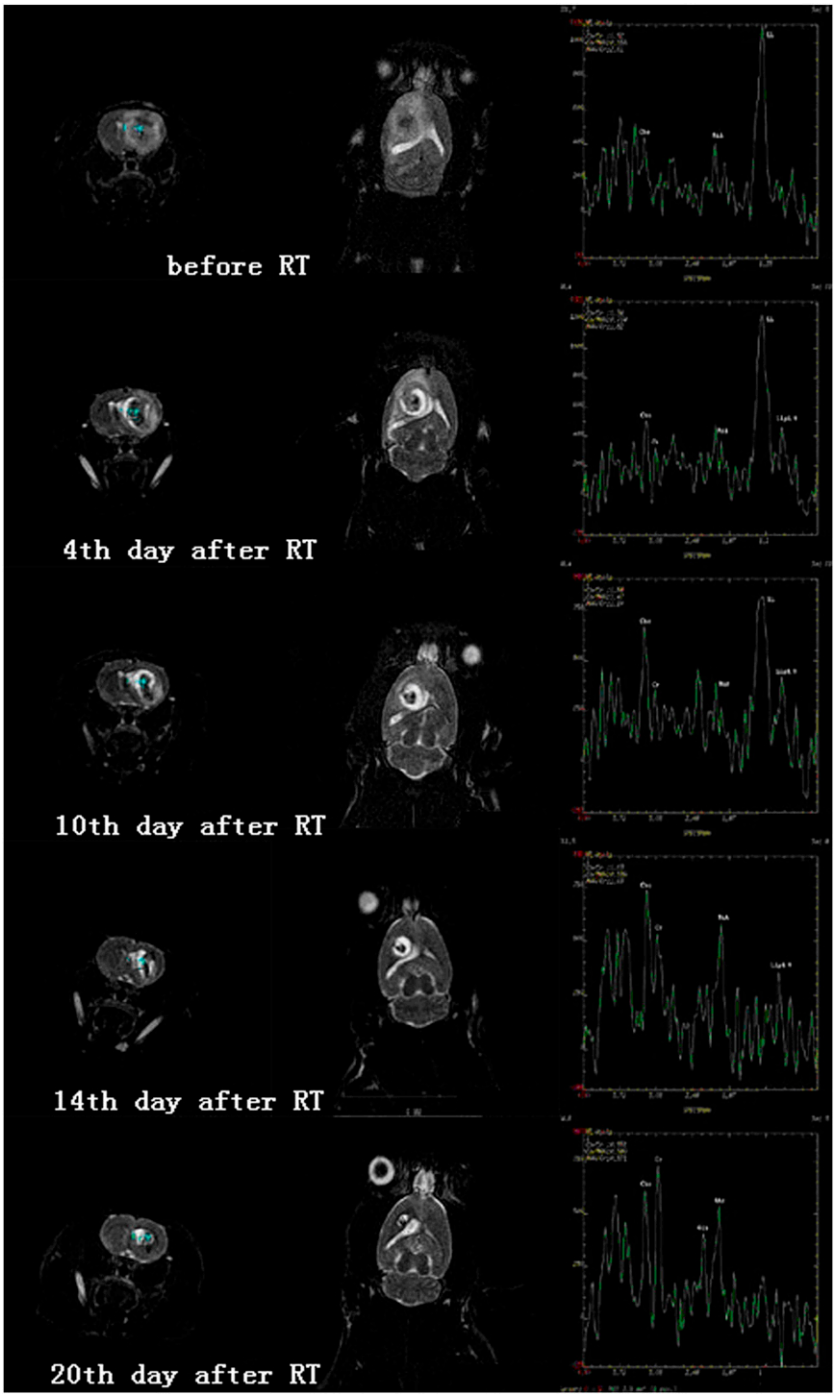

MRS was acquired prior to RT and on the 4th, 10th, 14th and 20th day after the treatment. GE FuncTool 2.6.4b software (GE Healthcare) was used to process the raw data that were stored in a workstation.

Tumour volume measurement

On the 18th day after C6 glioma cell injection, conventional MRI and MRS were used to observe the tumour volume and metabolic information. Volumetric measurement was implemented by manually contouring the tumour border on every slice using GE FuncTool software. The percentage change of tumour volume is defined as $(V_b - V_a)/V_a \times 100\%$, where V_a and V_b are tumour volumes measured before and after RT, respectively.

Ki-67 labelling index

For pathology and Ki-67 immunohistochemical staining, the intact skulls were removed and fixed in 10% paraformaldehyde solution. All procedures were performed under IP anaesthesia. Ki-67 LI is the

Table 2. Metabolic ratios estimated by MR spectroscopy before and after radiation therapy (RT)

Time relative to RT initiation	Cho/Cr, mean ± SD	Cho/NAA, mean ± SD	NAA/Cr, mean ± SD	Lip0.9/Cr, mean ± SD	Lipid and lactate/Cr, mean ± SD	mI/Cr, mean ± SD	Glutamate plus glutamine/Cr, mean ± SD
Prior to RT	1.71 ± 0.32	1.20 ± 0.24	1.49 ± 0.40	0.60 ± 0.27	2.18 ± 1.91	1.44 ± 0.44	0.92 ± 0.35
4 days	1.49 ± 0.55	1.24 ± 0.29	1.17 ± 0.33	0.76 ± 0.51	1.71 ± 1.67	1.39 ± 0.42	0.90 ± 0.45
10 days	1.15 ± 0.39[a]	0.99 ± 0.22	1.16 ± 0.20	0.43 ± 0.35	0.70 ± 0.57	1.12 ± 0.38	0.71 ± 0.15
14 days	0.92 ± 0.17[a]	0.86 ± 0.14[a]	1.09 ± 0.24	0.35 ± 0.15	0.53 ± 0.32	1.13 ± 0.28	0.63 ± 0.12
20 days	0.80 ± 0.17[a]	0.77 ± 0.23[a]	1.06 ± 0.16[a]	0.31 ± 0.14	0.52 ± 0.24	0.99 ± 0.16	0.60 ± 0.12

Cho, choline-containing components; Cr, creatine and creatine phosphate; Lip0.9, lipid signal at 0.9 ppm; ml, myo-inositol; NAA, *N*-acetyl aspartate; SD, standard deviation.
[a]Significant difference ($p < 0.01$).

percentage of Ki-67-positive nuclei in the total number of tumour cell nuclei per reference area. The tissue sample nearest to the spectroscopic voxel was visually identified through comparison with MR images and selected for the Ki-67 staining. The technique used for Ki-67 staining of paraffin-embedded sections was described by Shi et al.[30] The sections were deparaffinized, placed in 300 ml of citrate buffer with a pH of 6.0 and heated five times for 3 min each at full power in a 500-W microwave oven so as to activate the epitope of Ki-67 protein. After heating, the sections were reacted with mindbomb homologue 1 (MIB-1) diluted 1:50 in phosphate-buffered saline containing 1% normal rabbit serum and counter-stained with methyl green. >1000 cells were counted in several areas representative of the pathological characteristics, and the Ki-67 LI was calculated as the percentage of positively stained nuclei.

Biostatistical methods

Quantitative data analysis was performed using SPSS® v. 19 (SPSS Inc., Chicago, IL). All of the data are presented as means ± standard deviation (SD). The parameters in the two groups before and after RT were compared using repeated measures analysis of variance test, with $p < 0.05$ considered to be statistical significant. Pearson's correlation was used to indicate the relationship between two variables.

Receiver operating characteristics (ROC) analysis was used to determine a cut-off value for Cho/Cr and its power of outcome prediction was evaluated with Kaplan–Meier log-rank test.

RESULTS

In the 12 rats, it was found that the glioma cells were successfully growing into tumours in these healthy rats, which showed in conventional MRI and MRS images on the 18th day after cell injection. The tumour volume was evaluated by T_2 weighted MRI and the average tumour volume was 272 mm^3 for these 12 rats. Of the 12, 9 volumes reduced on Day 4 after RT, as shown in Table 1. Figure 2 shows the tumour volume change before and

Figure 3. The change in metabolic ratios before and after radiation therapy (RT). Cho, choline-containing components; Cr, creatine and creatine phosphate; Glx, glutamate plus glutamine; LL, lipid and lactate; NAA, *N*-acetyl aspartate.

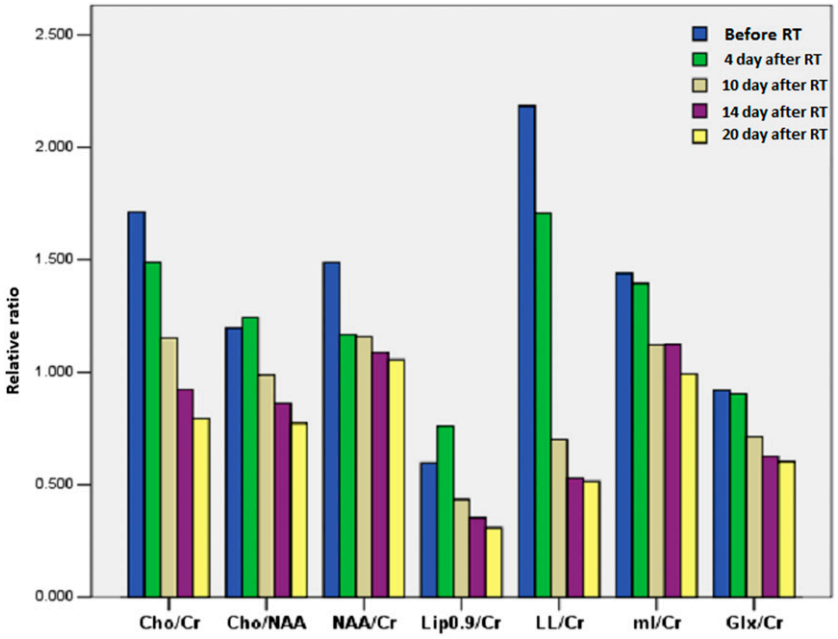

Figure 4. The relative tumour volume *vs* (a) Cho/Cr, (b) LL/Cr and (c) Glx/Cr, respectively. Cho, choline-containing components; Cr, creatine and creatine phosphate; Glx, glutamate plus glutamine; LL, lipid and lactate.

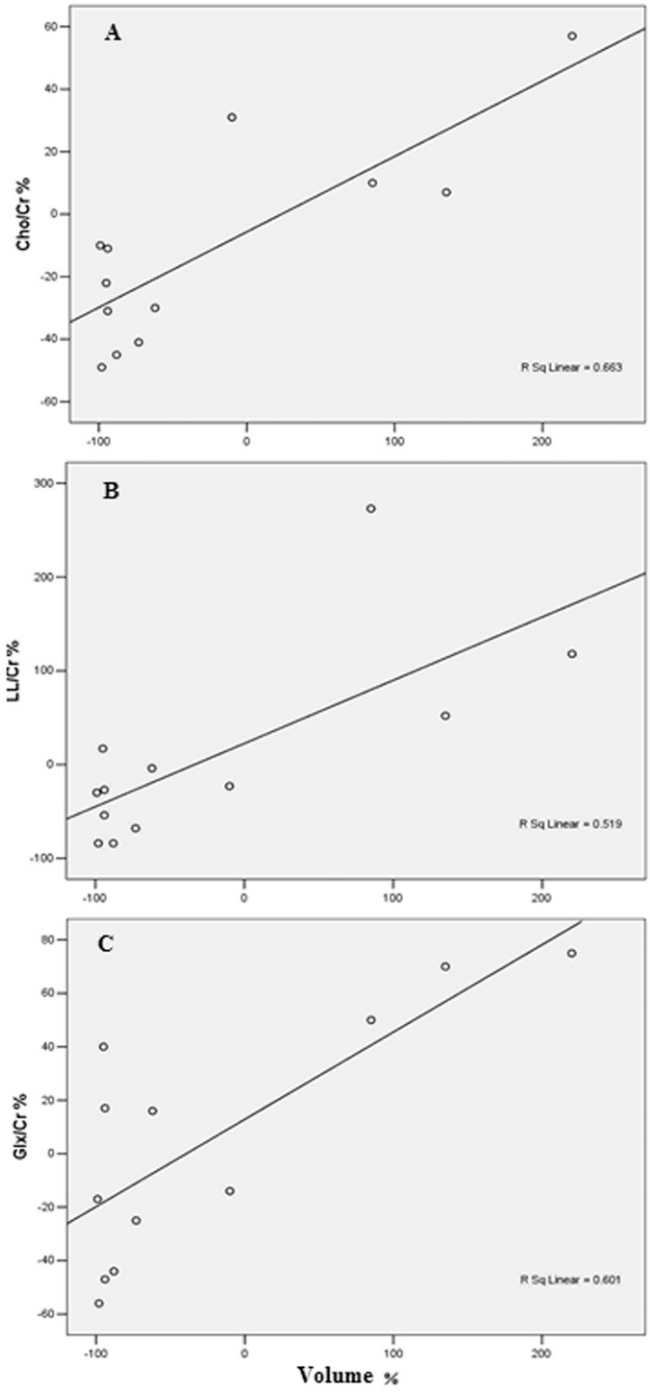

after RT. However, in the early phase of RT, three volumes corresponding to rat 1, 6, 12, respectively, were observed to increase at the fourth day after RT and decrease afterwards. The metabolic ratios evaluated by serial MRS after RT decreased progressively as a function of time after RT, as shown in Table 2. The metabolic ratios changed significantly sometime after RT as compared with those prior to RT, as shown in Figure 3.

The metabolic ratios for three rats were found to increase and then decrease. The change in the metabolic ratios remains consistent with the change in the tumour volume. Because there were tumour volume increases in three rats at the early phase of RT, it is necessary to record the metabolic changes. Table 1 summarizes the change in tumour volume and metabolic ratios including Cho/Cr, Cho/NAA, NAA/Cr, Lip/Cr, LL/Cr, myo-inositol (mI)/Cr and Glx/Cr for 12 rats at fourth day after RT. Pearson correlations showed a significant correlation between tumour volume and the metabolic ratios. For instance, tumour volume significantly correlated with Cho/Cr ($r = 0.814$; $p = 0.001$), LL/Cr ($r = 0.72$; $p = 0.008$) and Glx/Cr ($r = 0.775$; $p = 0.003$), respectively. Figure 4 plots the relative volume *vs* Cho/Cr, LL/Cr and Glx/Cr, respectively, showing that a linear relationship exists.

Cho/Cr, LL/Cr and Glx/Cr are independent variables for identifying the change of tumour volumes. At Day 4 after RT, the ROC analysis for the changes in Cho/Cr, LL/Cr and Glx/Cr showed that the areas under the curve were 0.926, 1.000 and 1.000, respectively, and the optimal values were −1.5%, 6.5% and 45.0%, respectively. These optimal values are able to identify whether tumour volumes increase. For instance, the optimal value of 45% in Glx/Cr can be used to separate tumour volumes into two groups with the tumour volume increasing in one group corresponding to the change of Glx/Cr >45% and the tumour volume decreasing in the other group. These three parameters were significantly correlated with tumour volumes ($p = 0.033$, 0.013 and 0.013, respectively) as shown in Table 3. A new variable was created that was the multiplication of three parameters (=Cho/Cr × LL/Cr × Glx/Cr) and was correlated with tumour volumes. When these three parameters were combined, the predictive power of tumour volume change was strengthened ($p = 0.012$) because of synergistic effect.

It has been found that there is a linear relationship between Ki-67 LI and the Cho/Cr ratio through Pearson correlations ($r = 0.85$; $p < 0.0001$), as shown in Figure 5a. Ki-67 LI has an average of 0.353, ranging from 0.038 to 0.749. Ki-67 LI decreases after RT as shown in Figure 6e,f and Figure 5b,c.

In a separate study with 62 rats of which 32 rats were injected with the same C6 tumour cells and 30 rats were used as a control group, our result of ROC analysis on Cho/Cr suggests that tumours might have a higher grade as Cho/Cr >2.0. Kaplan–Meier survival curves were obtained using the optimal value, as shown in Figure 7.

DISCUSSION

This animal model with C6 gliomas generated in rats provides great potential in studying tumour metabolites with MRS during RT. This study investigated the utility of MRS in the identification of brain astrocytic tumour biomarkers, providing useful information on using MRS biomarkers, such as NAA, Cho and LL for evaluating brain astrocytic tumours. NAA is recognized as an internal neural marker. It has a high peak in MRS of normal brains and tends to decrease in increasing malignant glioma.[31] In this study, it is interesting to observe that NAA decreases for 11 rats with increasing or decreasing volumes

Table 3. Area under the curve (AUC) through receiver operating characteristics analysis on the fourth day after radiation therapy

Variable	Cho/Cr	Cho/NAA	NAA/Cr	Lip0.9/Cr	Lipid and lactate/Cr	mI/Cr	Glutamate plus glutamine/Cr
AUC	0.926	0.704	0.759	0.815	1.000	0.630	1.000
p-value	0.033	0.309	0.196	0.116	0.013	0.518	0.013
95% CI	0.77–1.00	0.41–0.99	0.43–1.00	0.56–1.00	1.00–1.00	0.22–1.00	1.00–1.00

Cho, choline-containing components; CI, confidence interval; Cr, creatine and creatine phosphate; Lip0.9, lipid signal at 0.9 ppm; mI, myo-inositol; NAA, *N*-acetyl aspartate.

during RT. NAA decrease might reflect the fact that the neurons had been replaced by neoplasm, resulting in a decrease in the number of neurons and thereby a decline in the signal. However, for Rat 12, NAA/Cr increases as the tumour volume increases. This might be associated with oedema and thereby increasing neurons. In contrast to NAA, in astrocytomas, some investigators reported that Cho signal intensities always increase at a higher rate during more rapid development of neoplasm.[2] Other investigators pointed out that Cho peak actually has three components that cannot be resolved with magnetic fields <3 T.[13] Our results obtained by using a 3-T MRI scanner show that Cho levels increase with increasing tumour volume, in large parts owing to the increasing proliferation rate and denser cellular density. Cho/Cr decreases as tumour volumes decrease during RT. This might be explained by the fact that the metabolic rate decreases and therefore proliferation rate reduces during RT, which shows that Cho/Cr can be used to indicate tumour response to RT.

In astrocytomas, the relationship between the tumour grade and Cho levels exists with high-grade tumours having higher Cho levels. This can be explained by higher membrane turnover in aggressive tumours. However, it has been found that high-grade tumours have lower Cho levels than do grade I or grade II astrocytoma.[32] This is due to the presence of necrosis in high-grade tumours, which is associated with lower metabolites.[33] High Cho levels are typically observed in non-necrotic high-grade brain tumours, for example, anaplastic astrocytoma.[4]

Figure 5. Correlation of choline-containing components (Cho)/creatine and creatine phosphate (Cr) and Ki-67 labelling index (a) and change of Ki-67 labelling index haematoxylin and eosin stain after radiation therapy (RT) (b) and after RT (c).

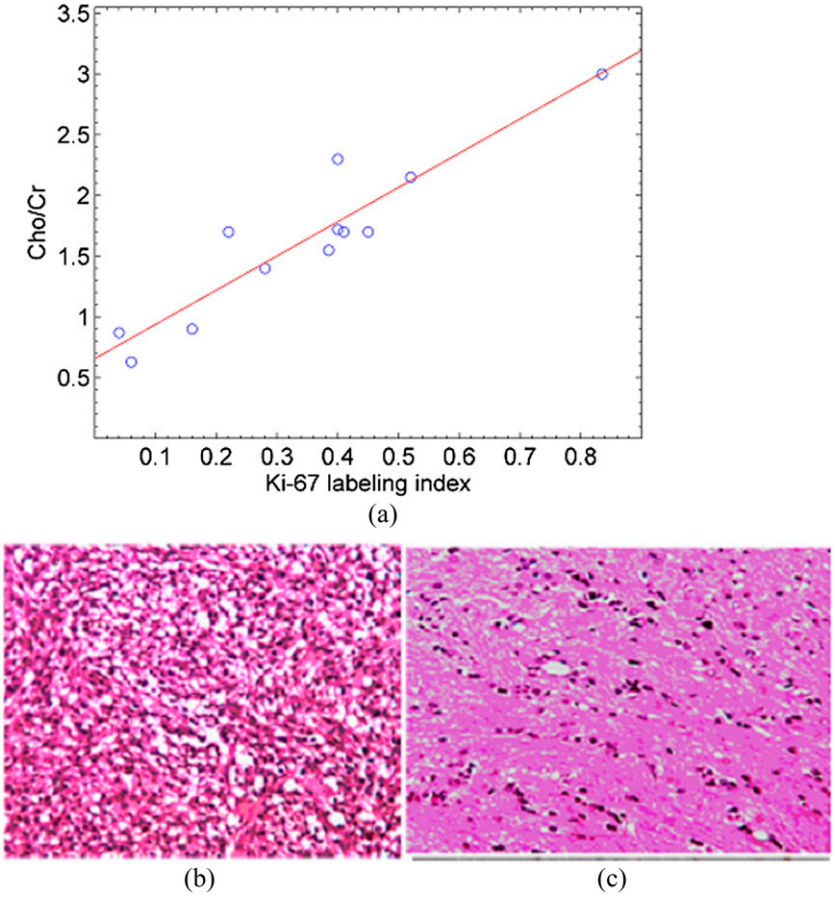

Figure 6. Spectrum changes on the fourth day after radiation therapy (RT) with lactate increasing dramatically as tumour volume increases. (a) MRI before RT; (b) MR spectroscopy (MRS) before RT; (c) MRI after RT; (d) MRS after RT; Ki-67 labelling index (e) haematoxylin and eosin stain afer RT and (f) after RT.

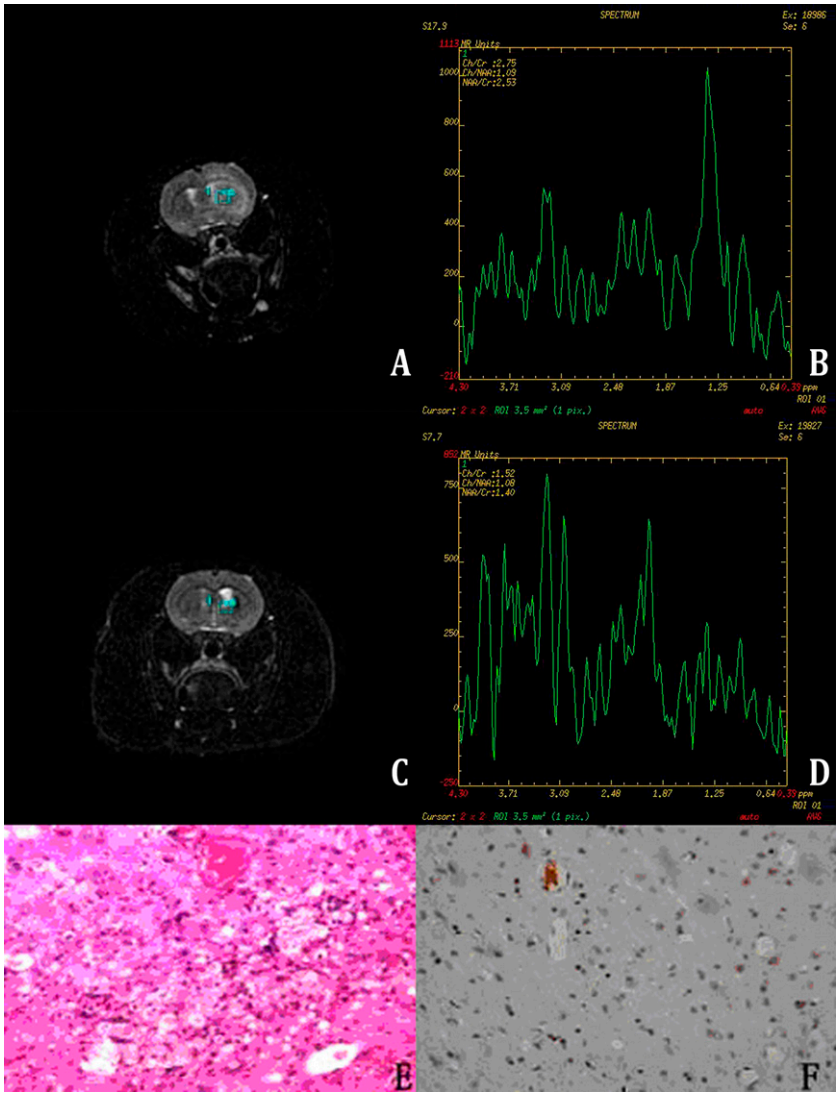

12 rats injected with C6 tumour cells grew into different grades that were correlated with Cho levels. ROC analysis on Cho levels provides an optimal value for classification of grades because of the significant correlation between Cho and tumour grades.[31,34] As shown in Figure 7, it turns out that the lifetime of a rat group with Cho/Cr ≤ 2 is longer than that with Cho/Cr >2, indicating the significant correlation ($p = 0.015$) between survival and Cho levels in the association with the tumour grade.

Lipid (at 1.3 ppm) and/or lactate (LL) peaks consist primarily of lactate and secondarily of lipid because our methodology focused on sensitization of lactate over lipid. Low LL signal is associated with low-grade gliomas that are generally characterized by a relatively high concentration of NAA, low Cho level and the absence of LL.[34] LL signal seems higher in grade IV and remains low in grade II or III gliomas[34,35] and the presence of lipid signal indicates the necrosis and lipid storage inside the gliomas.[36] Increased LL signal predicts high-grade brain tumours, which generally contain a high degree of necrosis.[13] Visible lipids in MRS correlate with necrosis, which cannot be differentiated from late-stage apoptosis through standard histology. Therefore, such a correlation by MRS provides useful prognostic information on the tumour grade.

The Glx peaks are defined between 2.15 and 2.45 ppm. Glx changes arise from both neuronal and glial cells and reflect cytoplasmic concentrations,[20] thus Glx can be used as an intercellular neurotransmitter marker. In our study, we observed that the tumour volume increased when Glx/Cr was >45% and decreased when Glx/Cr was <45%. This gives us evidence that Glx/Cr may be considered as a possible predictor of malignity degree of brain tumours.

Brain tumours are usually heterogeneous with necrotic cores, proliferative rims and invasion of surrounding tissues. The spectrum of MRS may vary from one region to another. Because of lesion variability, tumour heterogeneity, dependence on data

Figure 7. Kaplan–Meier survival analysis for choline-containing components (Cho)/creatine and creatine phosphate (Cr) ($p = 0.015$).

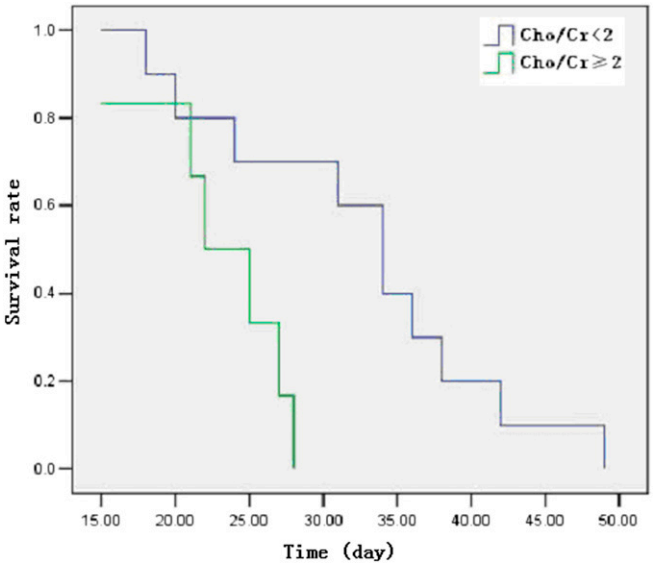

acquisition and analysis techniques, it is very difficult to use MRS alone to precisely diagnose a brain lesion. In this case, MRI should be combined together with MRS. It is important to locate a region of interest for sophisticated analysis. Heterogeneous spectroscopic voxels through MR images normally indicate high Ki-67 LI, whereas homogeneous spectroscopic voxels present low Ki-67 LI.[15] After RT, Ki-67 LI decreases, as shown in Figure 5b,c. This might be explained by the fact that tumour perfusion status improves through RT and tumour volume decreases,[37] and hence the status of tumour heterogeneity changes.

MRS findings should be interpreted with caution because they vary greatly with the time from brain injury to scan and also vary with the patient's age.[14] For example, NAA levels in the normal brain increase rapidly during maturation, reach a maximum around 10–15 years of age, and then decline slowly owing to the decreased number of neurons.[14] Although NAA/Cr ratios have remained similar across studies, results should be interpreted cautiously because differences in the underlying pathophysiological mechanisms were observed in experimental data with the same NAA/Cr ratios. Our experimental design overcomes the time variation in MRS studies because of the same time scheme was used for the 12 rats at the same age.

In this study, the tumour volume varied from one rat to another. The partial volume averaging may affect the accurate determination in the tumour volume. As the tumour volume was becoming small, the partial volume artefact would make it difficult to delineate the tumour border. The main strategy for decreasing partial volume artefacts is to use smaller, more sharply defined voxels. This means thinner sections, smaller FOV and/or higher imaging matrix.

MRS is a very useful technique that allows the investigation of biochemical pathology within the brain, including brain tumours during RT, and provides reproducible diagnostic and prognostic biomarkers for evaluating tumour biology and metabolism. Our results suggest that the normalized Cho and lactate correlate strongly with tumour volume change after RT, which is an important prognostic factor for clinical outcome.

REFERENCES

1. Cancer facts and figure 2014. American Cancer Society, Atlanta, GA; 2014. Available from: www.cancer.org
2. Chen J, Huang SL, Li T, Chen XL. *In vivo* research in astrocytoma cell proliferation with 1H-magnetic resonance spectroscopy: correlation with histopathology and immunohistochemistry. *Neuroradiology* 2006; **48**: 312–18.
3. Nano R, Lascialfari A, Corti M, Paolini A, Pasi F, Corbella F, et al. New frontiers for astrocytic tumours. *Anticancer Res* 2012; **32**: 2755–8.
4. Horská A, Barker PB. Imaging of brain tumors: MR spectroscopy and metabolic imaging. *Neuroimaging Clin N Am* 2010; **20**: 293–310. doi: 10.1016/j.nic.2010.04.003
5. Triscott J, Lee C, Foster C, Manoranjan B, Pambid MR, Berns R, et al. Personalizing the treatment of pediatric medulloblastoma: polo-like kinase 1 as a molecular target in high-risk children. *Cancer Res* 2013; **73**: 6734–44. doi: 10.1158/0008-5472.CAN-12-4331
6. Nutt CL, Mani DR, Betensky RA, Tamayo P, Cairncross JG, Ladd C, et al. Gene expression-based classification of malignant gliomas correlates better with survival than histological classification. *Cancer Res* 2003; **63**: 1602–7.
7. Magalhaes A, Godfrey W, Shen Y, Hu J, Smith W. Proton magnetic resonance spectroscopy of brain tumors correlated with pathology. *Acad Radiol* 2005; **12**: 51–7.
8. Signoretti S, Marmarou A, Fatouros P, Hoyle R, Beaumont A, Sawauchi S, et al. Application of chemical shift imaging for measurement of NAA in head injured patients. *Acta Neurochir Suppl* 2002; **81**: 373–5.
9. Holshouser BA, Tong KA, Ashwal S. Proton MR spectroscopic imaging depicts diffuse axonal injury in children with traumatic brain injury. *AJNR Am J Neuroradiol* 2005; **26**: 1276–85.
10. Holshouser BA, Tong KA, Ashwal S, Oyoyo U, Ghamsary M, Saunders D, et al. Prospective longitudinal proton magnetic resonance spectroscopic imaging in adult traumatic brain injury. *J Magn Reson Imaging* 2006; **24**: 33–40.
11. Belanger HG, Vanderploeg RD, Curtiss G, Warden DL. Recent neuroimaging techniques in mild traumatic brain injury. *J Neuropsychiatry Clin Neurosci* 2007; **19**: 5–20.
12. Govind V, Gold S, Kaliannan K, Saigal G, Falcone S, Arheart KL, et al. Whole-brain proton MR spectroscopic imaging of mild-to-moderate traumatic brain injury and correlation with neuropsychological deficits. *J Neurotrauma* 2010; **27**: 483–96. doi: 10.1089/neu.2009.1159
13. Astrakas LG, Zurakowski D, Tzika AA, Zarifi MK, Anthony DC, De Girolami U, et al. Noninvasive magnetic resonance spectroscopic imaging biomarkers to predict the clinical grade of pediatric

brain tumors. *Clin Cancer Res* 2004; **10**: 8220–8.
14. Shekdar K, Wang DJ. Role of magnetic resonance spectroscopy in evaluation of congenital/developmental brain abnormalities. *Semin Ultrasound CT MR* 2011; **32**: 510–38. doi: 10.1053/j.sult.2011.08.001
15. Shimizu H, Kumabe T, Shirane R, Yoshimoto T. Correlation between choline level measured by proton MR spectroscopy and Ki-67 labeling index in gliomas. *AJNR Am J Neuroradiol* 2000; **21**: 659–65.
16. Croteau D, Scarpace L, Hearshen D, Gutierrez J, Fisher JL, Rock JP, et al. Correlation between magnetic resonance spectroscopy imaging and image-guided biopsies: semiquantitative and qualitative histopathological analyses of patients with untreated glioma. *Neurosurgery* 2001; **49**: 823–9.
17. Signoretti S, Di Pietro V, Vagnozzi R, Lazzarino G, Amorini AM, Belli A, et al. Transient alterations of creatine, creatine phosphate, N-acetylaspartate and high-energy phosphates after mild traumatic brain injury in the rat. *Mol Cell Biochem* 2010; **333**: 269–77. doi: 10.1007/s11010-009-0228-9
18. Rock JP, Hearshen D, Scarpace L, Croteau D, Gutierrez J, Fisher JL, et al. Correlations between magnetic resonance spectroscopy and image-guided histopathology, with special attention to radiation necrosis. *Neurosurgery* 2002; **51**: 912–19; discussion 19–20.
19. Marcus KJ, Astrakas LG, Zurakowski D, Zarifi MK, Mintzopoulos D, Poussaint TY, et al. Predicting survival of children with CNS tumors using proton magnetic resonance spectroscopic imaging biomarkers. *Int J Oncol* 2007; **30**: 651–7.
20. Maddock RJ, Buonocore MH. MR spectroscopic studies of the brain in psychiatric disorders. *Curr Top Behav Neurosci* 2012; **11**: 199–251.
21. Ricci R, Bacci A, Tugnoli V, Battaglia S, Maffei M, Agati R, et al. Metabolic findings on 3T 1H-MR spectroscopy in peritumoral brain edema. *AJNR Am J Neuroradiol* 2007; **28**: 1287–91.
22. Calvar JA, Meli FJ, Romero C, Calcagno ML, Yánez P, Martinez AR, et al. Characterization of brain tumors by MRS, DWI and Ki-67 labeling index. *J Neurooncol* 2005; **72**: 273–80.
23. Kraguljac NV, White DM, Reid MA, Lahti AC. Increased hippocampal glutamate and volumetric deficits in unmedicated patients with schizophrenia. *JAMA Psychiatry* 2013; **70**: 1294–302. doi: 10.1001/jamapsychiatry.2013.2437
24. Barbarella G, Ricci R, Pirini G, Tugnoli V, Tosi MR, Bertoluzza A, et al. *In vivo* single voxel 1H MRS of glial brain tumors: correlation with tissue histology and *in vitro* MRS. *Int J Oncol* 1998; **12**: 461–8.
25. Bruna J, Brell M, Ferrer I, Gimenez-Bonafe P, Tortosa A. Ki-67 proliferative index predicts clinical outcome in patients with atypical or anaplastic meningioma. *Neuropathology* 2007; **27**: 114–20.
26. Fusco A, Zatelli MC, Bianchi A, Cimino V, Tilaro L, Veltri F, et al. Prognostic significance of the Ki-67 labeling index in growth hormone-secreting pituitary adenomas. *J Clin Endocrinol Metab* 2008; **93**: 2746–50. doi: 10.1210/jc.2008-0126
27. Turkoglu E, Kertmen H, Sanli AM, Onder E, Gunaydin A, Gurses L, et al. Clinical outcome of adult choroid plexus tumors: retrospective analysis of a single institute. *Acta Neurochir (Wien)* 2014; **156**: 1461–8. doi: 10.1007/s00701-014-2138-1
28. Pereira RS, Schweigert A, Dias de Melo G, Fernandes FV, Sueiro FA, Machado GF. Ki-67 labeling in canine perianal glands neoplasms: a novel approach for immunohistological diagnostic and prognostic. *BMC Vet Res* 2013; **9**: 83. doi: 10.1186/1746-6148-9-83
29. Ozawa T, Faddegon BA, Hu LJ, Bollen AW, Lamborn KR, Deen DF. Response of intracerebral human glioblastoma xenografts to multifraction radiation exposures. *Int J Radiat Oncol Biol Phys* 2006; **66**: 263–70.
30. Shi SR, Key ME, Kalra KL. Antigen retrieval in formalin-fixed, paraffin-embedded tissues: an enhancement method for immunohistochemical staining based on microwave oven heating of tissue sections. *J Histochem Cytochem* 1991; **39**: 741–8.
31. Izumiyama H, Abe T, Tanioka D, Fukuda A, Kunii N. Clinicopathological examination of glioma by proton magnetic resonance spectroscopy background. *Brain Tumor Pathol* 2004; **21**: 39–46.
32. Howe FA, Barton SJ, Cudlip SA, Stubbs M, Saunders DE, Murphy M, et al. Metabolic profiles of human brain tumors using quantitative *in vivo* 1H magnetic resonance spectroscopy. *Magn Reson Med* 2003; **49**: 223–32.
33. Sankar T, Caramanos Z, Assina R, Villemure JG, Leblanc R, Langleben A, et al. Prospective serial proton MR spectroscopic assessment of response to tamoxifen for recurrent malignant glioma. *J Neurooncol* 2008; **90**: 63–76. doi: 10.1007/s11060-008-9632-3
34. Bulik M, Jancalek R, Vanicek J, Skoch A, Mechl M. Potential of MR spectroscopy for assessment of glioma grading. *Clin Neurol Neurosurg* 2013; **115**: 146–53. doi: 10.1016/j.clineuro.2012.11.002
35. Kaminogo M, Ishimaru H, Morikawa M, Ochi M, Ushijima R, Tani M, et al. Diagnostic potential of short echo time MR spectroscopy of gliomas with single-voxel and point-resolved spatially localised proton spectroscopy of brain. *Neuroradiology* 2001; **43**: 353–63.
36. Zoula S, Hérigault G, Ziegler A, Farion R, Décorps M, Rémy C. Correlation between the occurrence of 1H-MRS lipid signal, necrosis and lipid droplets during C6 rat glioma development. *NMR Biomed* 2003; **16**: 199–212.
37. Sedlacik J, Winchell A, Kocak M, Loeffler RB, Broniscer A, Hillenbrand CM. MR imaging assessment of tumor perfusion and 3D segmented volume at baseline, during treatment, and at tumor progression in children with newly diagnosed diffuse intrinsic pontine glioma. *AJNR Am J Neuroradiol* 2013; **34**: 1450–5. doi: 10.3174/ajnr.A3421